NanoImpact 15 (2019) 100176

Contents lists available at ScienceDirect

NanoImpact

journal homepage: www.elsevier.com/locate/nanoimpact

A 21-day sub-acute, whole-body inhalation exposure to printer-emitted engineered nanoparticles in rats: Exploring pulmonary and systemic effects

Sandra V. Pirela[a,1], Kunal Bhattacharya[a,1], Yun Wang[b,1], Yipei Zhang[a], Guanghe Wang[a], Costas A. Christophi[c], John Godleski[a], Treye Thomas[d], Yong Qian[e], Marlene S. Orandle[e], Jennifer D. Sisler[e], Dhimiter Bello[a], Vincent Castranova[f], Philip Demokritou[a,*]

[a] Department of Environmental Health, Center for Nanotechnology and Nanotoxicology, T.H. Chan School of Public Health, Harvard University, Boston, MA, United States
[b] Department of Occupational and Environmental Health Sciences, School of Public Health, Peking University, Beijing, PR China
[c] Cyprus International Institute for Environmental and Public Health, Cyprus University of Technology, Limassol, Cyprus
[d] U.S. Consumer Product Safety Commission, Office of Hazard Identification and Reduction, Rockville, MD, United States
[e] Pathology and Physiology Research Branch, Health Effects Laboratory Division, National Institute for Occupational Safety and Health, Morgantown, WV, United States
[f] Department of Pharmaceutical Sciences, Mary Babb Randolph Cancer Center, West Virginia University, Morgantown, WV, United States

ARTICLE INFO

Editor: Bernd Nowack

Keywords:
Laser printer emissions
Engineered nanoparticles
Lung
Inflammation
Oxidative stress
Exposure biology

ABSTRACT

Engineered nanomaterials (ENMs) used in toners to improve their performance are released in the air during laser printer use. ENMs play an important catalytic role in the breakdown of the toner polymer and subsequent rearrangement of organic compounds as well as in the formation of reactive oxygen species (ROS). Cellular, animal, and human occupational exposure studies have shown that such printer-emitted particles (PEPs) induce inflammation, systemic oxidative stress, and genotoxicity, as well as, increase frequency of coughing, wheezing, and upper airway symptoms, raising concerns about their long-term impact on human health. No safety thresholds or regulatory guidelines currently exist for PEPs. In this study, Sprague-Dawley rats were exposed (by whole-body inhalation) to PEPs 5 h/day for up to 21 days using an exposure platform previously developed by the authors. The control group comprised of an equal number of rats exposed to high-efficiency particulate air (HEPA) filtered air. The PEPs had a mean particle diameter of approximately 45 nm, and a total particle number concentration ranging from 4 to 21 $\times 10^5$ #/cm^3. The maximum total volatile organic compound (tVOCs) concentration was 363.2 ± 162 ppb. The Multiple-Path Particle Dosimetry Model (MPPD) estimated the deposited fraction of PEPs to be around 7, 6 and 21% in the head, tracheobronchial (TB) and alveolar regions, respectively. Analysis of biochemical markers in the nasal and bronchoalveolar lavage fluids (NLF, BALF) of PEPs-exposed animals showed only mild oxidative stress and inflammation. No damage was detected in the histological and chemiluminescence analysis of lung and heart tissues of PEPs-exposed animals. Pro- and anti-inflammatory cytokines and chemokines, such as Interleukin (IL) 1β, IL-12, IL-18, MIP-1α, MIP-2, GRO/KC, and Fractalkine were found to be up-/down-regulated in NLF and BALF of the PEPs-exposed animals. Also, serum biomarkers of oxidative stress and inflammation, such as 8-isoprostane, 4-hydroxynonemal, and Leukotriene B4 were elevated in PEPs-exposed animals. In conclusion, following exposure to PEPs, there was modest lung injury and inflammation in the respiratory tract. Specifically, changes in expression of certain cytokines and chemokines, along with serum levels of 8-isoprostane, were the most significant adverse effects reported following exposure to PEPs.

1. Introduction

Engineered nanomaterials (ENMs) are introduced into a wide range of commercial products to improve their quality and functionality (Pyrgiotakis et al., 2016; Servin and White, 2016; McClements et al., 2016; Eleftheriadou et al., 2017; Schoepf et al., 2017; DeLoid et al., 2017; Yao et al., 2017; Eleftheriadou et al., 2017; DeLoid et al., 2018; Vaze et al., 2018; Sohal et al., 2018a; Sohal et al., 2018b). During the

* Corresponding author at: Department of Environmental Health, Center for Nanotechnology and Nanotoxicology, T. H. Chan School of Public Health, Harvard University, 665 Huntington Avenue, Room 1310, Boston, MA 02115, United States.
E-mail address: pdemokri@hsph.harvard.edu (P. Demokritou).
[1] Equally-contributing authors.

https://doi.org/10.1016/j.impact.2019.100176
Received 9 February 2019; Received in revised form 2 July 2019; Accepted 4 July 2019
Available online 10 July 2019
2452-0748/

lifecycle of these nano-enabled products, such as product manufacturing, utilization and disposal, ENMs can be released in the environment and come in direct contact with humans (Pal et al., 2015; Sotiriou et al., 2015; Wohlleben and Neubauer, 2016; Sotiriou et al., 2016; Watson-Wright et al., 2017; Singh et al., 2017).

Early physicochemical characterization studies done on laser printer and photocopier toners have shown them to contain metallic ENMs made of iron oxide, titanium dioxide (TiO_2), silicon dioxide, aluminum oxide, zinc oxide (ZnO), copper oxide, and manganese oxide (Bello et al., 2013; Martin et al., 2015; Pirela et al., 2014; Pirela et al., 2015). During printing processes, these metallic ENM additives become airborne (called printer emitted particles, PEPs) and can reach levels > 1.4 million #/cm^3 in various photocopy centers (Martin et al., 2015; Pirela et al., 2017). The PEPs are comprised primarily of particulate matter with aerodynamic diameters of < 100 nm ($PM_{0.1}$), accounting for up to 8% of the $PM_{0.1}$ composition (Pirela et al., 2017; Martin et al., 2015). Additionally, the ENMs contain organic derivatives formed during the thermal decomposition of toner polymers (Bello et al., 2013; Pirela et al., 2014; Scungio et al., 2017). Recently, Chalbot et al. followed the distribution of 16 Environmental Protection Agency–priority polyaromatic hydrocarbons (PAHs) in toners and airborne $PM_{0.1}$, and documented a shift from low molecular weight PAHs (naphthalene, acenaphthylene and acenaphthene) present on the surface of PEPs to more carcinogenic high molecular PAHs (chrysene, anthracene and benzo[*a*]pyrene) (Chalbot et al., 2017). This effect was attributed to the catalytic effect of ENMs in toners.

The presence of several nanoscale transition metals/metal oxides in PEPs together with other organic compounds, raises concerns over potentially significant cellular damage in the deep airways, as well as translocation into the interstitial space, circulatory system and lymphatic vessels (due to their small size), from where they may be distributed throughout the body (Kreyling et al., 2017; Miller et al., 2017; Oberdorster et al., 2005). While translocation and clearance kinetics of some metal oxides (TiO_2, ZnO) present in PEPs have been studied in animals (Kreyling et al., 2017 for TiO_2; Konduru et al., 2014 for ZnO), the biokinetics and translocation of PEPs has not.

The bioactivity of PEPs has been documented by the authors and others using both *in vitro* and *in vivo* models. In a comprehensive review on the topic, Pirela et al. have demonstrated that PEPs are capable of inducing a range of adverse biological responses (Pirela et al., 2017). PEPs were found to induce cell damage and death through the production of reactive oxygen species (ROS), oxidative stress, inflammatory responses, and modulation of DNA methylation in epigenetic mechanisms under *in vitro* conditions in human small airway epithelial cells, microvascular endothelial cells, macrophages, and lymphoblasts (Pirela et al., 2016b; Sisler et al., 2015; Lu et al., 2015). *In vivo* murine instillation studies have also demonstrated that PEPs in whole lung tissues can (1) induce up-regulation of pro-inflammatory cells such as neutrophils and macrophages; (2) increase the expression of pro-inflammatory genes (Nos1, Ccl5 and Ucp2) and of TE LINE-1; and, (3) enhance mitochondrial membrane instability, a significant loss of DNA methyltransferase Dnmt3a (Lu et al., 2016; Pirela et al., 2016a, 2016b).

The few available acute human exposures and epidemiological studies conducted in photocopy centers (also reviewed comprehensively in Pirela et al., 2017; Khatri et al., 2017) have documented similar biomolecular and organ function responses in humans to those previously observed in *in vitro* and laboratory animal studies. Workers exposed to PEPs at photocopier centers in India were found to have a high prevalence of nasal blockage, cough, excessive sputum production, and breathing difficulties in addition to elevated markers for oxidative stress and lower albumin to globulin ratios (Elango et al., 2013). Khatri et al. (2013a, 2013b, 2013c) reported the exposure-related time course changes of upper airway inflammation and systemic oxidative stress in healthy volunteers exposed for 5 h in a copy center, as well as chronic upper airway inflammation and oxidative stress in a small group of chronically exposed copy center workers (Khatri et al., 2017). Additional studies have shown the induction of oxidative stress through production of ROS and reduced transfer capacity for nitric oxide, as well as inflammatory responses, reduced lung capacity and translocation of PEPs into the sub-mesothelium in lungs of humans exposed to PEPs (Theegarten et al., 2010; Khatri et al., 2013a, 2013b, 2013c; Karimi et al., 2016; Yang and Haung, 2008; Awodele et al., 2015).

The main objective of the present study was to document the impact of PEPs exposures on the cardiovascular system, and the deep lung functions of rodents in a 21-day sub-acute whole-body inhalation exposure study. Rodents were exposed to PEPs for 5 h a day for up to 21 consecutive days. Control animals were exposed to high efficiency particulate air (HEPA) filtered air. Real-time expsoure assessment of PEPs and VOCs was performed. $PM_{0.1}$ deposited and retained, after an estimated cleared fraction was subtracted, in the lungs of rodents was calculated using (MPPD) model (v3.0, Anjilvel and Asgharian, 1995). A diverse set of biochemical and histological markers were generated covering the lungs and the circulatory system. Dose response relationships were derived and used to estimate the no and lowest observable adverse effects levels for respiratory effects (*i.e.*, NOAEL and LOAEL) in rodents.

2. Materials and methods

2.1. Animals

One hundred thirty-four 9-week old Sprague-Dawley healthy male rats, weighing an average of 300 g, were purchased from Taconic Farms Inc. (Hudson, NY). The rats were allowed to acclimatize for 1 week before the studies were initiated. Baseline data (rat body weight) were collected for 1 week before the exposures occurred. The rats were maintained on a 12-hour light/dark cycle and food and water were provided *ad libitum*. Upon arrival, animals were randomly assigned a unique identification number, which determines the exposure group for the animal. There were two treatment groups: a) Control group: (HEPA) filtered air, and b) PEPs Exposure group. All the animals were treated humanely in accordance with the guiding principles on the Use of Animals in Toxicology and the Animal Care and Use Committee of Harvard University (Ethical permit No. 04623).

2.2. Whole-body inhalation exposure of animals and collection of biological samples

The exposed group consisted of animals housed in individual cages and exposed *via* whole-body inhalation to PEPs and gaseous pollutants emitted by laser printer B1 using the Printer Exposure Generation System (PEGS) described in detail in a previous publication (Pirela et al., 2014) (Fig. 1). In summary, printer B1 was used to generate PEPs emissions by printing a 5%-page coverage monochrome document using standardized settings (Pirela et al., 2014). The laser printer B1 was selected based on exposure profiles reported in our previous studies (Pirela et al., 2014). In parallel, another group of animals was exposed to HEPA-filtered air. The system was configured for 12 chambers (one animal per chamber), each equipped with a port for aerosol delivery and temperature and humidity measurement, a water bottle port, and a gas sampling port.

The whole-body exposure experiment was repeated twice, in 2016 and 2017. Animals were placed in their chambers for 1–5 h for 5 days prior to the exposures to ensure they gradually acclimated to the exposure chambers before the exposures occurred. The following week, animals were exposed to PEPs pollutants and the room HEPA-filtered air 5 h/day for up to 21 consecutive days. The exposure duration of 21 days, as well as the sacrifice time points, were chosen as a sub-acute exposure period to provide several delivered doses to the lung and identify any signs of toxicity in the cardiovascular or respiratory systems.

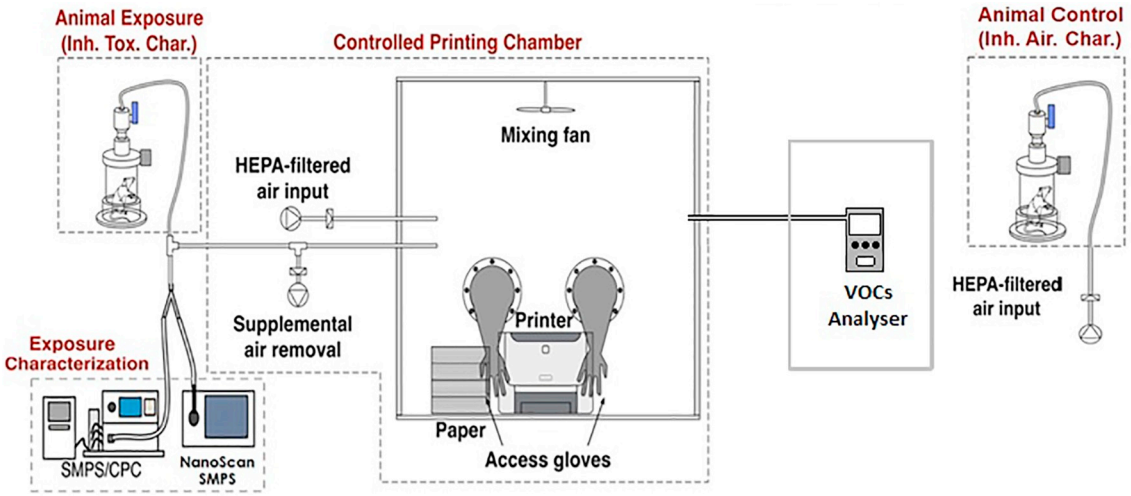

Fig. 1. Printer Exposure Generation System (PEGS). The exposure platform for whole-body inhalation experiment and exposure characterization of PEPs from an emitting laser printer.

Please note that a group of animals was selected to undergo chemiluminescence analysis on the first and fifth day of exposure. Another group of animals was selected to obtain tissue sections that were stained for a quantitative and qualitative assessment of inflammation based on white blood cell population and presence of any particles, in addition to histopathological changes induced by PEPs exposure.

2.3. Collection of nasal lavage fluid (NLF) and biochemical assay

At the completion of each exposure period (2016: day 1 (L1), day 5 (L5), day 9 (L9), day 13 (L13), day 17 (L17), and day 21 (L21); and 2017: day 1 (R1), day 5 (R5), day 9 (R9), day13 (R13), day 17 (R17), and day 21 (R21)), the animals in each particular group were anesthetized with an intraperitoneal injection of a lethal dose (200 mg/kg) of pentobarbital sodium (Anthony Products Co., Arcadia, CA) and sacrificed by exsanguination, followed by nasal lavage fluid (NLF) and bronchoalveolar lavage fluid (BALF) collections.

The nasal passages were lavaged *in situ* twice with 0.75 mL of sterile saline. Both washes were pooled for biochemical assays. Cells were separated from the supernatant in all washes (400 $\times g$ at 40 °C for 10 min). Total and differential cell counts, as well as hemoglobin (Hb) measurements were made from the cell pellets. Total cell counts were performed manually using a hemocytometer. Cell smears were made with a cytocentrifuge (Shandon Southern Instruments, Inc., Sewickley, PA) and stained with Diff-Quick (American Scientific Products, McGaw Park, IL). Differential cell counts were performed by counting 200 cells per animal. The supernatant fraction of the first two washes was clarified by sedimentation at 15,000 $\times g$ for 30 min and used for enzyme activity, albumin and cytokine measurements. For the enzymatic and spectroscopic assay all the reagents were purchased from Sigma-Aldrich, St. Louis, MO. The lactate dehydrogenase (LDH), peroxidase activity, albumin, Hb and total glutathione (GSH) levels in NLF and BALF were tested using previously published spectrophotometric assays and quantified using specific standards (Beck et al., 1982). Briefly, LDH was assayed by following the oxidation of NADH in the presence of pyruvate at 340 nm. One unit equals one micromole of substrate converted per minute at 25 °C. Peroxidase activity was measured spectrophotometrically at 470 nm by monitoring the oxidation of guaiacol to tetraguaiacol in the presence of H_2O_2. One unit equals an increase in absorbance of 1.0 per minute. Albumin was determined by measuring the binding of the dye bromocresol green at 630 nm with bovine serum albumin as a standard (Doumas et al., 1971). Total cellular glutathione (GSH) level was measured using GSH-Glo™ Glutathione assay (Promega, Madison, WI). The assay is based on the detection of luminescence reflecting the conversion of a luciferin derivative into luciferin in the presence of glutathione; the reaction is catalyzed by glutathione s-transferase.

2.4. Collection of BALF and biochemical assay

At each sacrifice time point immediately following the nasal lavage, a bronchoalveolar lavage was performed. The lungs were lavaged *in situ* with two washes of 4 mL of sterile saline. The washes were pooled for biochemical assays. Cells were separated from the supernatant in all washes (400 $\times g$ at 40 °C for 10 min). Total and differential cell counts, as well as Hb measurements were made from the cell pellets. Total cell counts were performed manually using a hemocytometer. Cell smears were made with a cytocentrifuge (Shandon Southern Instruments, Inc., Sewickley, PA) and stained with Diff-Quick (American Scientific Products, McGaw Park, IL). Differential cell counts were performed by counting 200 cells per animal. The supernatant fraction of the first two washes was clarified by sedimentation at 15,000 $\times g$ for 30 min and used for enzyme activity, albumin and cytokine measurements. For the enzymatic and spectroscopic assays, all reagents were purchased from Sigma-Aldrich, St. Louis, MO. Standard spectrophotometric assays for detecting LDH, peroxidase activity, albumin, and Hb levels used in the nasal lavage study were applied in the BALF study (Beck et al., 1982).

2.5. Multiplex cytokine analysis

Cytokine levels in NLF and BALF collected from animals from different exposure durations (2016: L1, L5, L9, L13, L17 and L21; and, 2017: R1, R5, R9, R13, R17 and R21) were measured by Eve Technologies Corporation (Calgary, Alberta, Canada) using a Rat Cytokine Array/Chemokine Array 27-Plex kit (Millipore, St. Charles, MO, USA) according to the manufacturer's protocol. The 27-plex consisted of eotaxin, EGF, Fractalkine, IFN-γ, IL-1α, IL-1β, IL-2, IL-4, IL-5, IL-6, IL-10, IL-12(p70), IL-13, IL-17α, IL-18, IP-10, GRO/KC, TNF-α, G-CSF, GM-CSF, MCP-1, Leptin, LIX, MIP-1α, MIP-2, RANTES, and VEGF. The sensitivities of the assay to these markers ranged from 0.3 to 63.6 pg/mL. Results were presented as fold changes in the levels of inflammatory mediators in NLF and BALF based on retention dose (μg/m^2) of the PEPs-exposed animals and compared to those of the HEPA filtered air-exposed control animals.

2.6. In situ reactive oxygen species measurement

In situ reactive oxygen species generation was measured in the

microvasculature of pulmonary and cardiac tissues using *in vivo* chemiluminescence method in a separate portion of animals that did not undergo NL or BAL (IVCL, Sotiriou et al., 2012). Briefly, after completion of the exposure period, control (n = 4) and PEPs-exposed (n = 4) animals were anesthetized with an intraperitoneal injection of a lethal dose (200 mg/kg) of pentobarbital sodium (Anthony Products Co., Arcadia, CA) and were placed on a heating pad to maintain homeostatic body temperature. The animals were surgically intubated using a 14G × 2″ catheter connected to a small animal respirator (Harvard Apparatus). The cardiac and pulmonary tissues were exposed *in situ* by median total sternotomy and by folding the rib cage aside laterally with the use of hemostats as retractors. A 2 × 2 gauze was then dampened and placed behind both the pulmonary and cardiac tissues to provide elevation above the plane of the animal. A light blocking material, with a hole in the center, was used for the exposure of the desired tissue (*i.e.*, beating heart). This non-reflecting sheet was then wrapped around the animal and it was placed in the chemiluminescence chamber (maintaining intubation, under anesthesia effect) to obtain tissue chemiluminescence levels for periods of 30 s. Then, the animal was removed and the light blocking material moved to only expose the right lung. Upon completion of the readings (photon measurements capture) the animal was euthanized, while anesthetized, by cutting the abdominal aorta, causing painless exsanguinations.

2.7. Sample preparation for serum analysis of 8-Isoprostane and Leukotriene B4 (LTB_4)

Tenng of the internal standards, 8-isoprostane-d_4 and LTB_4-d_4 (Cayman Chemical, Ann Arbor, MI, USA), were added to a 1 mL aliquot of the animal blood serum sample. Two mL of acetonitrile was added to the serum sample to denature proteins. The sample was stored in the refrigerator at 4 °C for 30 min and then centrifuged at 3000 rpm for 10 min to remove precipitated proteins. The supernatant was placed in a vacuum oven until dryness and reconstituted in 1 mL of 5% ammonium hydroxide in water prior to solid phase extraction (SPE).

For SPE, a strong anion polymeric SPE cartridge (Strata-X-A, 200 mg/3 mL; Phenomenex, Torrance, CA, USA) was used. The cartridge was preconditioned with 2 mL of methanol and equilibrated with 2 mL of 5% ammonium hydroxide in water. Then, the reconstituted serum sample from the previous step was loaded into the column, followed by a washing step consisting of 2 mL of 5% ammonium hydroxide in water and 2 mL of methanol. The analytes were eluted from the cartridge with 2 mL of 5% formic acid in methanol. The eluate was dried under vacuum, and resuspended in 200 µL of 20% methanol in water. The prepared samples were analyzed by liquid chromatography-electrospray ionization-tandem mass spectrometry (LC-ESI-MS/MS) as described later. Sample recovery was assessed in independent experiments.

2.8. Sample preparation for serum analysis for 4-Hydroxynonenal (4-HNE)

4-HNE, formed endogenously from lipid peroxidation, is an important biomarker of oxidative stress (Syslová et al., 2009). Because of the high reactivity of 4-HNE post-SPE sample processing, derivatization of 4-HNE with 2,4-dinitrophenylhydrazine (DNPH) was completed after SPE purification (described later), and prior to its analysis by LC-ESI-MS/MS (Douny et al., 2016).

1 ng of 4-HNE-d_3 internal standard (Cayman Chemical, Ann Arbor, MI, USA) was added to a 0.5-mL aliquot of animal blood serum samples followed by 1 mL of acetonitrile. The sample was then processed identically as in the case of LTB_4 to remove precipitated proteins. The supernatant was evaporated to dryness in a vacuum oven and reconstituted with 1 mL of deionized water.

Strata-X-A (Phenomenex) SPE was preconditioned with 2 mL of methanol and equilibrated with 2 mL of water. Then the reconstituted sample from the previous step was loaded onto the column, followed by a washing step with 2 mL of water. The analytes were eluted with 2 mL of acetonitrile. Then 4-HNE in the eluate was derivatized with DNPH. The derivatization protocol was based on a previous publication (Douny et al., 2016) with slight modifications. Briefly, 10 µL of DNPH solution (0.05 M in acetonitrile and acetic acid 9:1, v/v) was added into the sample eluate and standards, and placed in a water bath at 40 °C for 2 h. Then, the solution was dried under the vacuum and reconstituted in 200 µL of acetonitrile, followed by LC-ESI-MS/MS analysis for 4-HNE-DNPH and 4-HNE-d_3-DNPH derivatives.

2.9. Standard calibration for LC-ESI-MS/MS analysis

The stock solution of 8-isoprotane (10 µg/mL), LTB_4 (10 µg/mL), and 4-HNE (1 µg/mL) were prepared by dilution of standard with acetonitrile and stored at −80 °C. For 8-isoprostane and LTB_4, 9 concentrations were prepared from their respective stocks: 0.5, 1, 5, 10, 50, 100, 250 and 500 ng/mL. Ten ng each of 8-isoprostane-d_4 and LTB_4-d_4 were added to each of the standard solutions. The calibration curves for 8-isoprostane and LTB_4 were generated using the ratio of peak areas of the analyte (8-isoprostane or LTB_4) to its corresponding internal standard peak area (8-isoprostane-d_4 or LTB4-d_4) as a function of analyte concentration.

Eight concentrations (50 pg/mL-100 ng/mL) of 4-HNE standard solution were prepared by dilution from 4-HNE stock solution. 1 ng of 4-HNE-d_3 was spiked to the standard solution. Then, the 4-HNE and its internal standard were derivatized by DNPH as described previously. The calibration curve of 4-HNE was plotted based on the peak area ratios of 4-HNE-DNPH to the 4-HNE-d_3 peak area *versus* the concentration of 4-HNE.

Calibration curves, limit of detection and analyte recoveries are summarized in Supplemental Table S1. Excellent linear regression lines were obtained for all analytes ($R^2 > 0.999$) over the tested concentration range. Analyte recoveries were also satisfactory (91–96%) for all three analytes.

2.10. LC-ESI-MS/MS analysis of 8-isoprostane, LTB4 and 4-HNE-DNPH

LC-ESI-MS/MS analysis was conducted on a Shimadzu LC-20AD chromatographic system coupled with an API 3200 triple quadruple mass spectrometer equipped with a Turbo Ion Spray source (Applied Biosystems, Foster City, CA, USA). Electrospray ionization (ESI) was performed in the negative ion mode. Ion spray voltage was kept at −4500 V, the temperature of ion spray was set at 600 °C. Nitrogen was selected as the nebulizing, heater, curtain, and collision gas. The gas flow was optimized as follows: nebulizing at 65 psi, heater at 50 psi, and curtain gas at 30 psi.

For sample preparation and LC-ESI-MS/MS calibration the analytes 8-isoprostane, LTB_4 and 4-HNE and their corresponding deuterated internal standard were measured in the multiple reaction monitor mode (MRM). The MRM transition and MRM parameters for each analyte were studied and optimized by continual infusion of standard (10 µg/mL, flow 10 µL/min). Their MRM transitions and parameters are summarized in Supplemental Table S2. Chromatographic separation was achieved on a Kinetex polar-C18 column (4.6 × 150 mm, 2.6 µm particle size) (Phenomenex, Torrance, CA) at a flow rate of 600 µL/min, with a column temperature set at 40 °C. The mobile phase A was 0.1% ammonium hydroxide in water, mobile phase B was 0.1% ammonium hydroxide in methanol. A gradient elution was as follows: 25% B for the first two min, to 90% B at 12 min, in a linear gradient. Then the column was equilibrated at 25% B for 3 min. The sample injection volume was 10 µL. Duplicate injections were made for all samples.

In addition to NLF and BALF, heart, lungs and serum samples were obtained. Particularly, the lung and heart samples were evaluated *in vivo* for microvascular ROS generation by *in situ* chemiluminescence only on L1 and L5 of 2016 exposures using our previously developed method as discussed under Section 2.6 (Sotiriou et al., 2012). Lung and

heart tissues obtained from both the PEPs and HEPA air exposed animals were also studied histologically for inflammation and particle deposition following hematoxylin and eosin (H&E) staining.

2.11. Animal exposure characterization (PEPs and gaseous co-pollutants)

2.11.1. Real time measurements

Particle number concentration, size distribution, temperature, relative humidity and tVOC levels were measured in real time in one of the 12 animal inhalation exposure chambers throughout the exposure durations. A scanning mobility particle sizer (SMPS Model 3080, TSI Inc., Shoreview, MN) was also used for measuring particle number concentration and size distribution (ranging from 2.5 to 210 nm) in the chamber. Real time particle number concentration as a function of size collected by the SMPS were used to estimate the mass size distribution assuming spherical particles and the density of carbon. Real-time tVOC levels were also monitored using a tVOC monitor (Graywolf Sensing Solutions, Shelton, CT). All the real time instruments were calibrated, and background tests were performed at the beginning of each sampling experiment. No significant variation in the temperature (°C) and relative humidity (%) in the inhalation animal chambers was observed throughout the exposure period (Supplemental Table S3).

It is worth noting that a comprehensive chemical analysis was performed by the authors and described in detail in our previous publications (Pirela et al., 2015; Chalbot et al., 2017). In summary, PEPs possess a complex mixture of metals (1–33%) and primarily various organic compounds including PAHs (0.0067%) and other compounds such as elemental carbon (1–3%), organic carbon (42–89%). It is also worth noting that in a recent publication by the authors (Chalbot et al., 2017), it was documented that there are synergistic interactions of catalytic metallic nanoparticles with gaseous sVOCs co-pollutants which result in the formation of high molecular and carcinogenic PAHs on the surface of the PEPs.

2.11.2. In vivo dosimetry analysis

MPPD version 3.04 was used for determining the deposition dose of PEPs in three main regions of the rat's respiratory tract, namely the head, TB, and pulmonary (alveolar regions) (Anjilvel and Asgharian, 1995). Dosimetry modeling was done using the asymmetric Sprague-Dawley rat lung model with the body orientation set to lying on stomach. For extrapolating results to human exposure scenario, the Yeh-Schum 5-Lobe lung model with upright orientation was used for dosimetry calculations. Breathing scenario was defined as whole-body exposure for the rats and oro-nasal-normal augmenter for the human calculations and lung clearance with zero pause fraction was included as a parameter. The deposition dose was calculated using functional residual capacity (FRC), upper respiratory tract (URT), breathing frequency, tidal volume, and inspiratory fractions based on the animal's body weight (Supplemental Tables S4 and S5). Additionally, average values of the PEPs particle density, count median diameter (CMD), geometric standard deviation (GSD), and particle mass concentration values, obtained from real-time analysis of emissions from each of the exposure groups in the 2016 and 2017 21-day exposure studies, were applied in the MPPD rat model analysis (Supplemental Table S6). Similar for the human model, average values of the PEPs particle density, CMD, GSD, and particle mass concentration, obtained in the 2016 21-day exposure studies, were used in the MPPD analysis (CMD 49.0 nm, GSD 1.7, and particle mass concentration 76.4 $\mu g/m^3$). PEPs were assumed to be spherical nanoparticles, an assumption generally supported by electron microscopy observations. Results were presented as the deposition fraction (percentage), deposition mass flux, deposition mass per lung area, and retained mass of PEPs after lung clearance.

2.12. Statistical analysis

Data were expressed as means ± standard deviation (SD) and were presented using bar graphs for the different groups considered. Statistical comparisons between the exposure and control groups for all tested parameters were performed using the Wilcoxon sign ranked non-parametric test. The total deposited mass for each exposure duration group in the study and its association with each one of the outcomes considered in the study was assessed with the use of quantile (median) regression. Statistical Analysis Software (SAS) version 9.3 (SAS Institute, Cary, NC, USA) was used for the analysis. All tests performed were two-sided and P value ≤ 0.05 was considered statistically significant. Results obtained from the study were used for estimating the no observable adverse effect level (NOAEL) and the lowest observable adverse effect level (LOAEL) in rats and equivalent NOAEL and LOAEL doses in humans, assuming that a similar health effect as seen in rats would be observed in humans (Supplemental Tables S6 and S7; Oller and Oberdorster, 2010). Other parameters such as body weight, FRC volume, URT volume, breathing frequency, tidal volume and inspiratory factions are mentioned in Supplemental Table S4.

3. Results

3.1. Real-time animal exposure characterization

Individually caged 9-week-old Sprague-Dawley rats were exposed to laser printer B1 emitted particulates (PEPs) using our printer emission generation system (PEGS; Fig. 1; Pirela et al., 2014). Real-time measurements of the mean particle diameter (nm), particle number concentration ($10^5/cm^3$), particle mass concentration ($\mu g/m^3$), and count median diameter (nm) of PEPs from laser printer B1 are presented in Supplemental Table S8 and Fig. 2. All exposure subgroups in the year 2016 are labeled as L series, and those in 2017 as R series (Supplemental Table S8 and Fig. 2). One notable observation from Fig. 2(A and B) is that exposures in the 2016 series of experiments were more variable and higher than in the 2017 experiments. The size distributions were, however, similar. For example, the total number concentration during all exposure (L) sessions in 2016 varied between sessions from 5 to 21 $\times 10^5$ $\#/cm^3$, a four-fold range, whereas for the R series in 2017, the total particle number concentration was approximately 4–5 $\times 10^5$ $\#/cm^3$ (Supplemental Table S8 and Fig. 2; Pirela et al., 2014). PEPs size distributions were relatively constant across the 21-day exposure duration, with similar modal diameters and geometric standard deviations (GSD) between different sessions in 2016 and 2017 (Supplemental Table S8 and Fig. 2C–E). The highest mean particle diameter, particle mass, and number concentration was observed in the day 1, 2016 (L1) exposure group, with the following values: 67.6 ± 6.3 nm, 737.9 ± 137.6 $\mu g/m^3$, and 21.7 ± 3.9 $\times 10^5/cm^3$, respectively. These variations in each exposure day have been addressed *via* MPPD modeling of regional aerosol deposition (Supplemental Table S8).

Previous studies done in our group have shown the PEPs emitted by printer B1 are composed of a complex mixture of 50–90% organic carbon, 0.001–0.5% elemental carbon, 1–3% metals (Cu, Ce, Cr, Ni, Fe, and Ti), and low and high molecular weight PAHs (Pirela et al., 2015; Chalbot et al., 2017). Furthermore, the tVOCs analysis in the year 2016 showed VOCs to be present at relatively low concentrations, with daily averages between 244.8 ± 164.2 parts per billion (ppb) (L17) and 363.2 ± 161.7 ppb (L9) (Supplemental Table S8). The tVOCs during the 2017 sessions were not measured.

3.2. In vivo dosimetry considerations

The MPPD model deposited fraction of PEPs in the lungs of the rats was estimated to be around 7% in the head, 6% in the TB region and 21% in the alveolar region. The total deposition fraction ranged from32 to 35% in the 2016 and 2017 experiments, respectively. No significant change was observed in the deposition fraction of each exposure duration group (Fig. 3A and B). The deposited mass flux of the PEPs exhibited some variability consistent with variations in the particle

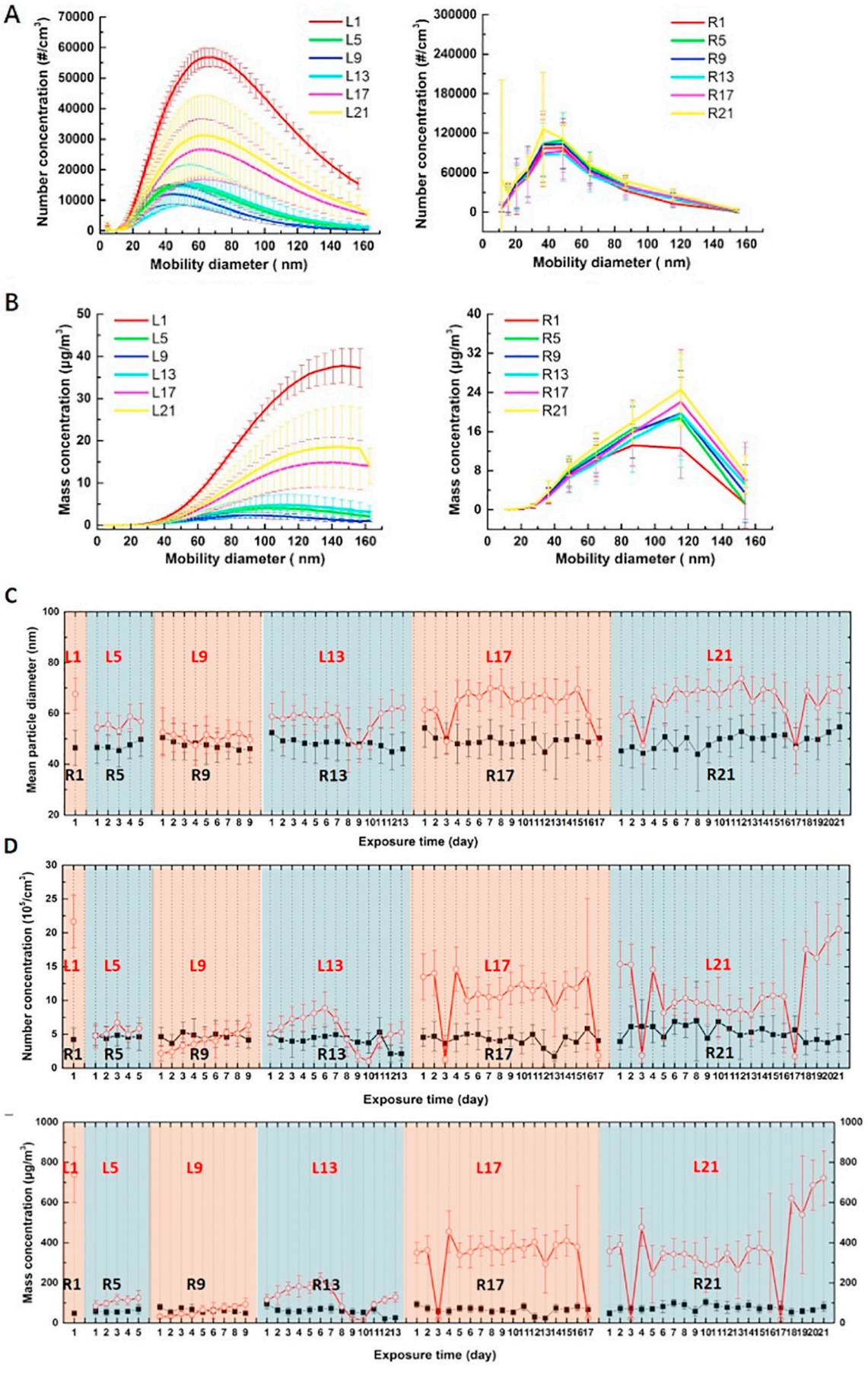

(caption on next page)

Fig. 2. Particle concentration and size distribution from the laser printer throughout the continuous inhalation exposure of PEPs for 1, 5, 9, 13, 17 and 21 days. (A) Particle number concentrations as a function of mobility diameter. (B) Particle mass concentrations as a function of mobility diameter. (C) Daily mean particle diameter during PEPs exposure in each experimental group. (D) Daily particle number concentrations during PEPs exposure in each experimental group. (E) Daily particle mass concentrations during PEPs exposure in each experimental group (mean ± SD). L1, L5, L9, L13, L17 and L21 in Fig. 2A–E represent results obtained in 2016 on days 1, 5, 9, 13, 17, and 21. Similarly, results obtained in 2017 on days 1, 5, 9, 13, 17, and 21 are marked as R1, R5, R9, R13, R17, R21. It should be noted that the large decrease in the daily particle diameter, mass, and number concentration in days L13, L17 and L21 (in 2016) was related to the use of another laser printer of the same brand instead of the damaged laser printer B1 in some days.

mass concentration (Fig. 3A and B, Supplemental Table S8). The estimated total particle mass deposition post clearance (retained mass) increased with exposure duration from 0.3 to 93.6 μg/m^2 (2016, L1 to L21) and 0.7–20.3 μg/m^2 (2017, R1 to R21) (Supplemental Table S9). When comparing the 2016 exposure sessions with 2017, the total retained mass of PEPs in day L21 was 4.5 times higher than the same exposure duration R21 group (Supplemental Table S9), which reflects differences in the aerosol concentrations between the 2016 and 2017 sessions. The highest pulmonary mass deposition and retention of PEPs in the alveolar region was estimated to be 110.4 μg and 91.9 μg, respectively, after 21 days of exposure in the 2016 study (L21) (Fig. 3B and C; Supplemental Table S9). Applying the estimated retention mass

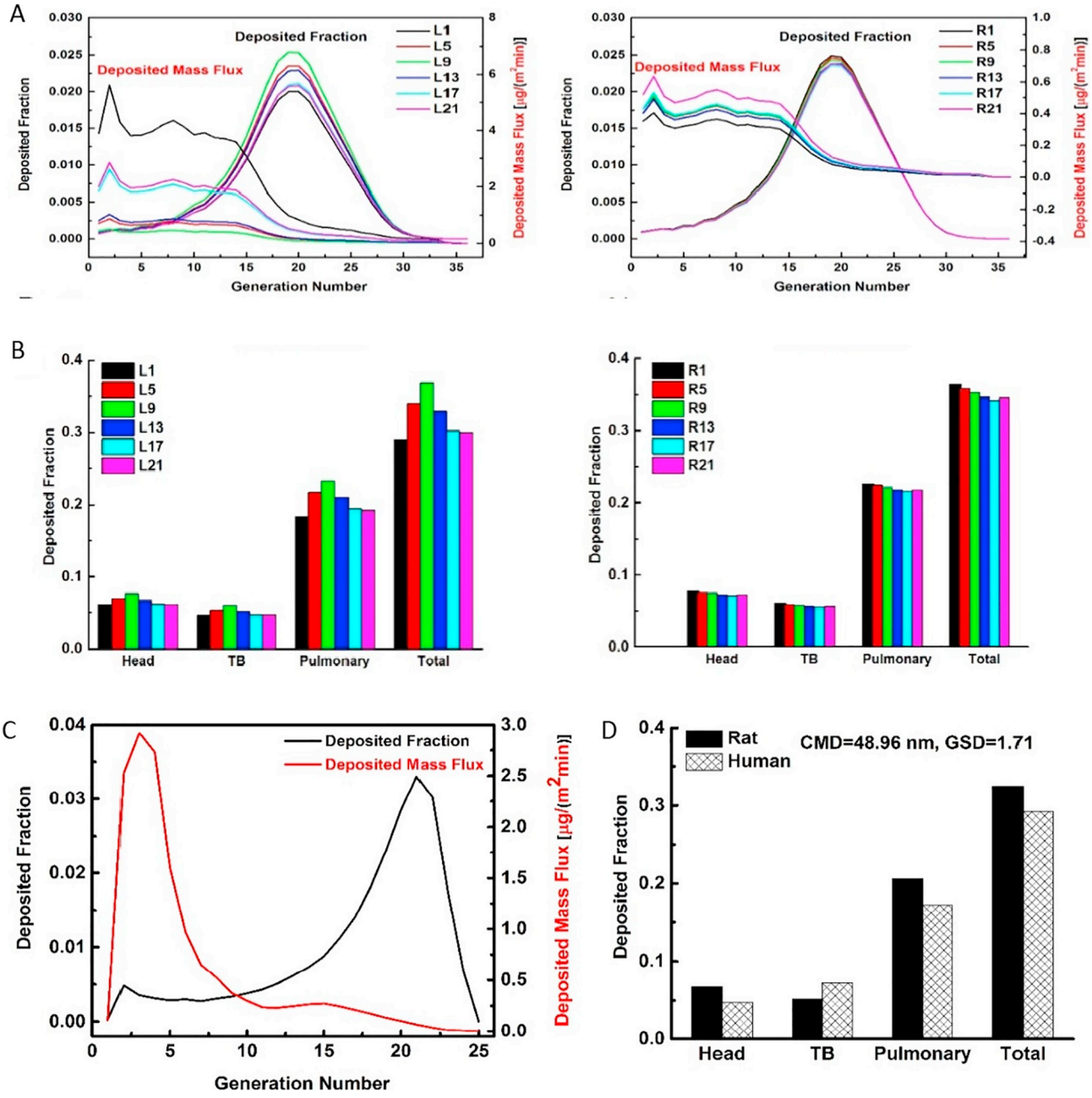

Fig. 3. Modeled deposition of PEPs in the rat and human airway. (A) Deposition fraction and deposition mass flux as a function of generation number of the rat airway. (B) Deposition fraction in head, the tracheobronchial and pulmonary sections of the rat airway, and total deposition. (C) Deposition fraction and deposition mass flux as a function of generation number of the human airway. (D) Deposition fraction in the head, tracheobronchial and pulmonary sections of the rat and human airway. TB, tracheobronchial regions; CMD, count median diameter; GSD, geometric standard deviation.

(μg) to the alveolar surface area of the Sprague-Dawley rats (0.29 m^2) (Jarabek et al., 2005; Pinkerton et al., 2015; Morfeld et al., 2015), the highest estimated PEPs retained dose on day 21 was 322.6 μg/m^2 (L21) and 70 μg/m^2 (R21) (Supplemental Table S9).

By extrapolating these estimates from rats to humans (in occupational settings or home office scenarios) working for 8 h per day, 5 days per week for 3 weeks, the total equivalent deposited fraction of PEPs in human lungs was estimated at 30% (Fig. 3D), a number similar to earlier estimates in humans based on realistic human monitoring data (Martin et al., 2015). It must be noted that non-occupational consumer exposures are expected to be less than in occupational settings. Similar to rats, the highest estimated deposition of PEPs for humans, from the aerosol exposures, was in the pulmonary region (Fig. 3D), with an estimated deposition mass of 2278.4 μg or 36.3 μg/m^2 of alveolar surface (Supplemental Table S9). The highest retained mass of PEPs in the alveolar region of humans was estimated at 1810 μg (Supplemental Table S9).

3.3. Biological responses: upper respiratory tract injury

Upper respiratory tract responses following exposure to PEPs were studied in 2016 using nasal lavage fluid (NLF) and by measuring biological end-points such as lactate dehydrogenase (LDH) release, total glutathione level (GSH), and peroxidase activity (Fig. 4). All the biological responses were normalized to the calculated retained dose (μg/m^2) of PEPs in the pulmonary region of the rats based on the real-time particulate matter measurements and MPPD model calculation. The obtained results showed that the PEPs retained in the pulmonary region (1.1–322.8 μg/m^2) did not induce release of LDH in the upper respiratory tract, with levels of LDH comparable to those present in the HEPA filtered air exposed control animals (Fig. 4A, Supplemental Fig. S1A). A modest PEPs induced dose-dependent increase was observed for NLF GSH and peroxidase concentrations; however, these changes were not statistically significant (Fig. 4B and C, Supplemental Fig. S1B and C).

3.4. Biological responses: lower respiratory tract injury

Lung injury was assessed in the bronchoalveolar lavage fluid (BALF) by measuring end-points such as LDH release, peroxidase activity, albumin, and Hb leakage into airways, total GSH levels and inflammatory cell infiltrates. These endpoints were expressed as a function of the retained dose (μg/m^2) in the deep airways, combining both 2016 and 2017 studies. Analysis of the BALF LDH release indicated mild cytotoxicity in the lower respiratory tract at the PEPs retained doses of 28.2 μg/m^2 (deposition rate: 0.4 μg/h; L5) and 79.3 μg/m^2 (deposition rate: 0.5 μg/h; L13) (P value ≤ 0.05) (Fig. 5A). No further changes in LDH levels were seen at the other retained doses (Fig. 5A, Supplemental Fig. S1D). Analysis of BALF peroxidase activity in the PEPs-exposed animals indicated no significant inflammatory responses in the pulmonary region of the animals, which was further substantiated by minimal neutrophil extravasation, and lack of significant accumulation of proteins (albumin), and damage to the integrity of the lung membrane (Figs. 5B and C, 6C, Supplemental Fig. S1E and F). Minor hemorrhage to the pulmonary region in the PEPs-exposed animals was observed through the presence of BALF Hb at the retained rate of 70 μg/m^2 after 21 days of exposure to PEPs in the 2017 study (R21) (P value ≤ 0.05) (Fig. 5D, Supplemental Fig. S2D). No further hemorrhage was observed in the PEPs exposed rats at the other retained doses. A minor, but not statistically significant, increase in the BALF total GSH levels was observed in the PEPs-exposed animals up to the retained dose of 252.1 μg/m^2 obtained after 17 days PEPs exposure in 2016 study (L17) (Fig. 5E, Supplemental Fig. S1H).

Analysis of inflammatory cells in the BALF of PEPs-exposed animals showed no significant change was detected in the white blood cell population (Fig. 6A). Using differential cell counting, the majority

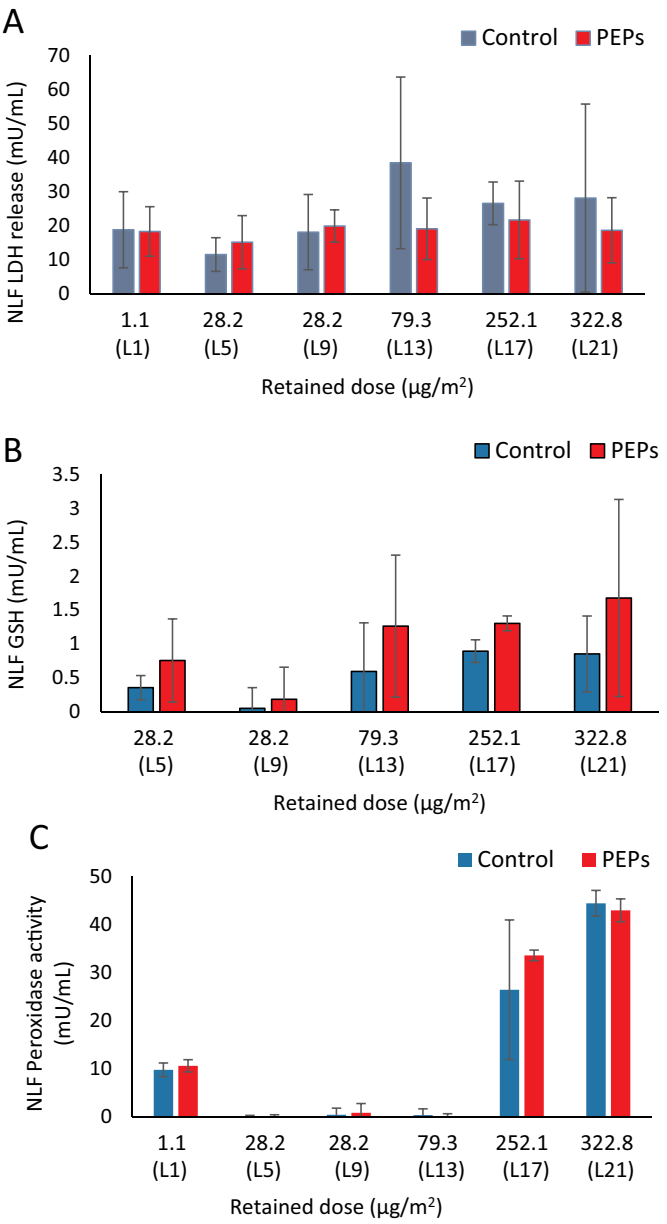

Fig. 4. Upper respiratory tract injury. Biological responses were studied in the nasal lavage fluid (NLF) collected from the rats exposed to HEPA filtered air (control) or PEPs, (A) Lactate dehydrogenase (LDH), (B) Total Glutathione (GSH) level, and (C) Peroxidase activity levels. Results obtained showed the absence of cytotoxic, inflammatory response or oxidative stress induction in the upper respiratory tract of the rats exposed to the PEPs up to the pulmonary retention dose of 322.8 μg/m^2. Results represent mean ± SD. For statistical analysis Wilcoxon sign ranked non-parametric test was performed.

(95%) of the cell population was found to be composed of macrophages. No significant changes in the inflammatory cell population were observed in the BALF of the PEPs-exposed animals throughout the 2016 and 2017 studies (Fig. 6A–D).

3.5. Multiplex analysis of inflammatory responses

Expression of pro- and anti-inflammatory cytokines, chemokines and growth factors were analyzed in the NLF and BALF of the PEPs-exposed animals and compared to those of the control HEPA filtered air exposed animals. NLF analysis of PEPs exposed animals showed >1-fold increase in the levels of three pro-inflammatory cytokines, IL-5, IL-12

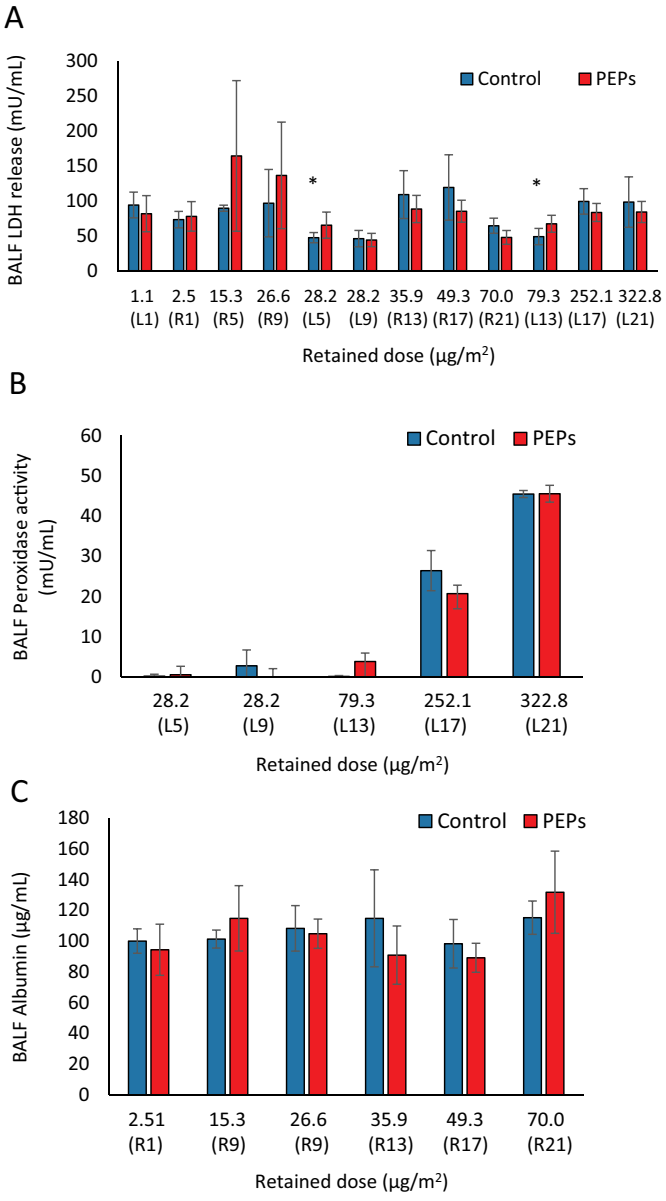

Fig. 5. Lower respiratory tract injury. Pulmonary injury in rats exposed to PEPs or HEPA filtered air (control) was studied in collected bronchoalveolar lavage fluid (BALF). Results were analyzed as a function a retention dose (μg/m^2) of PEPs and included: (A) Lactate dehydrogenase (LDH), (B) Peroxidase activity, (C) Albumin (μg/mL), (D) Hemoglobin, and (E) Glutathione (GSH). Only mild increases in injury markers were observed in the BALF obtained from the exposed rat. Results represent mean ± SD. For statistical analysis, Wilcoxon sign ranked non-parametric test was performed. P value * ≤ 0.05.

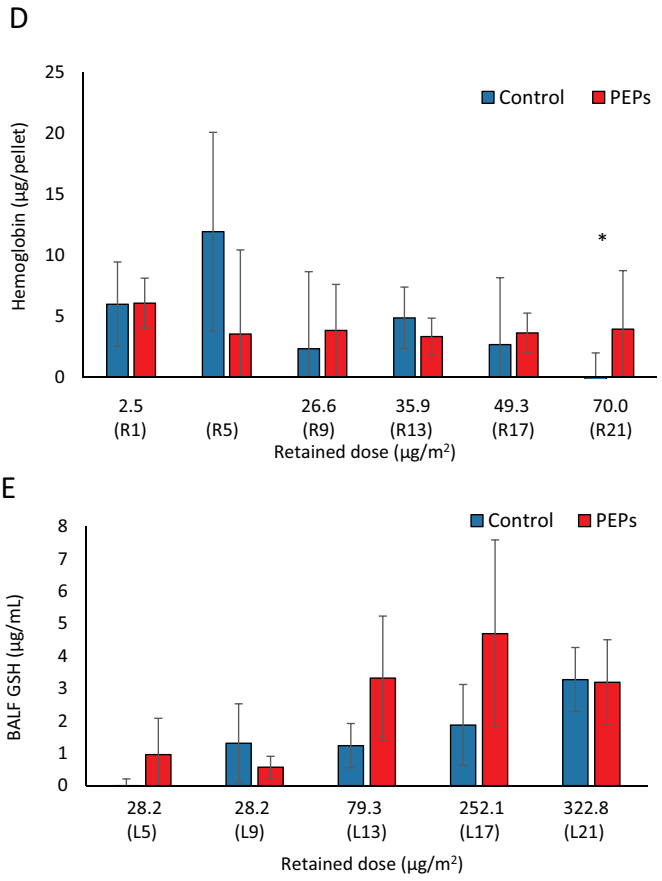

Fig. 5. (*continued*)

and IL-18 and growth factor protein VEGF beyond the retention dose of 35.9 μg/m^2 (R13) compared to control animals. Other inflammatory mediators such as, IL-1β, IL-17α, IFN-γ, Leptin, IL-13, MIP-1α, MIP-2, eotaxin, and GRO/KC were down-regulated in the NLF of the PEPs-exposed animals (Supplemental Fig. S2). In the BALF of PEPs-exposed animals, several pro- and anti-inflammatory mediators were found to be up-regulated, mostly up to the retention dose 28.2 μg/m^2 with the exception of IL-17α, IFN-γ and eotaxin showing down-regulation throughout the exposure (Supplemental Fig. S2). IL-18 up-regulation was only found to be statistically significant in the BALF at the retention dose of 28.2 μg/m^2 obtained after 5 days of exposure in the 2016 study (L5) (Supplemental Fig. S2). Up-regulation of pro-inflammatory mediators IL-1β, IL-18 and Fractalkine were found to be associated with increases in the deposited mass dose of PEPs in the exposed animals in multivariate regression analysis (Supplemental Figs. S1AE, S1AK, and S1AN).

It is worth noting that the minimum lung injury and inflammation results obtained from the current 2016 and 2017 studies are in agreement with the *in vitro* and *in vivo* instillation studies previously performed by the authors (Pirela et al., 2017).

3.6. Histopathological analysis of lungs and heart

H&E stained sections of lung and heart were evaluated from animals exposed to HEPA-filtered air (control) or to PEPs in the 2016 study. Animal tissue samples were obtained immediately after completion of exposure on L1, L5, L9, L13, L17 and L21. Several pulmonary abnormalities, such as small foci of type II pneumocyte hyperplasia, increased alveolar macrophages and a few neutrophils, and/or small numbers of eosinophils surrounding airways and blood vessels, were observed in the lung sections of both PEPs-exposed and control animals. Since these changes were minimal to mild in severity and were seen in both PEPs-exposed and control animals, this was considered non-specific background pathology. Particles were not seen in any sections examined. In the cardiac sections, some animals were found to have single, small foci of lymphocytic or granulomatous inflammation within the myocardium, but this is likely not a treatment-related finding as they were present in both PEPs-exposed and control animals.

3.7. In situ oxidative stress analysis in heart and lung tissues

Immediately after the last hour of exposure to PEPs and gaseous pollutants from the laser printer, the animals underwent *in situ* chemiluminescence reading in both the heart and the lungs. No significant

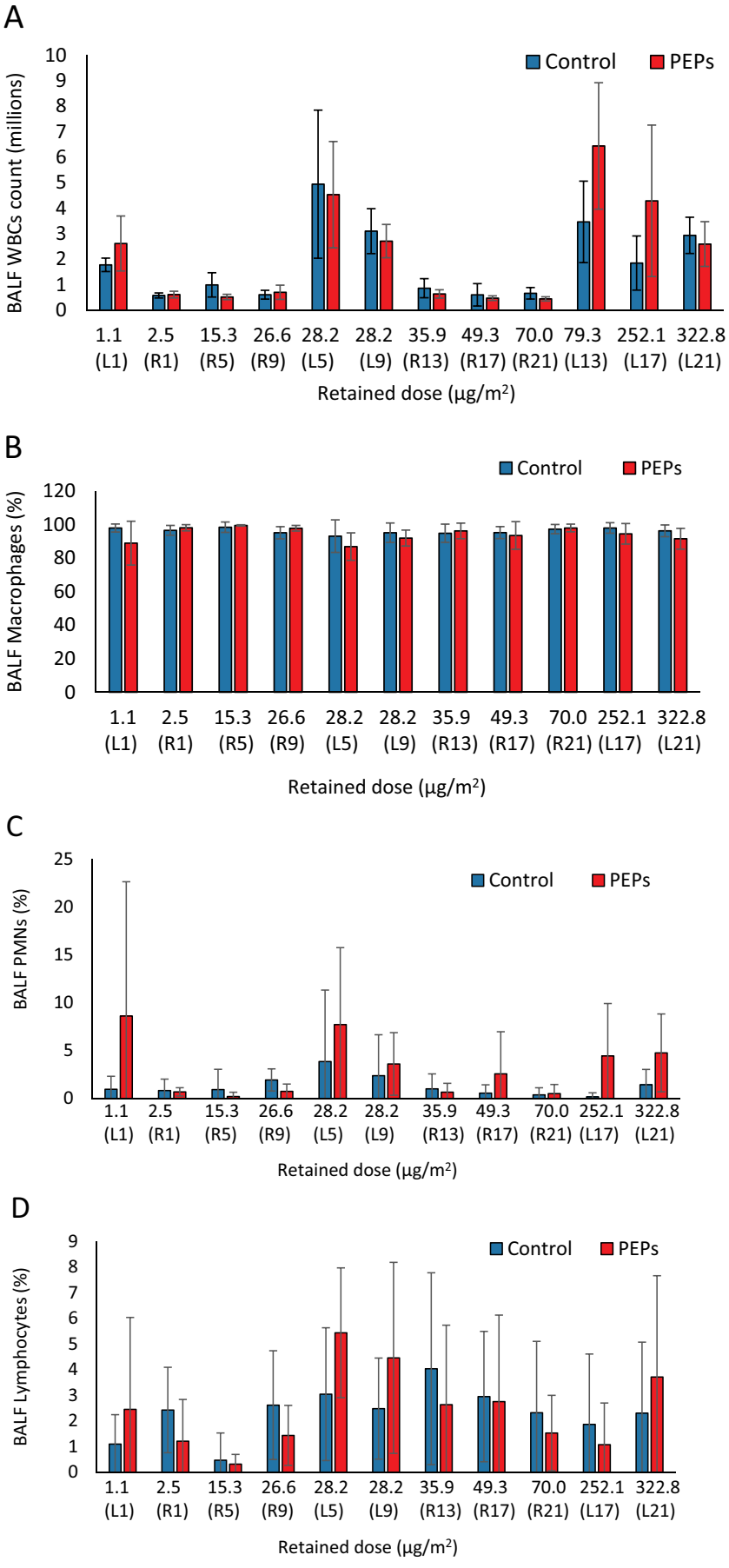

(caption on next page)

Fig. 6. Total and differential cell counts in rat bronchoalveolar lavage fluid (BALF). Total and differential cell counts were performed in the BALF of rats exposed to HEPA filtered air (control) or PEPs generated from a B1 laser printer. The results showed no change in the cell population of (A) white blood cell (WBC), (B) macrophages, (C) polymorphonuclear leukocytes (PMNs), and (D) lymphocytes, indicating no inflammatory response of the rats' lower respiratory tract to the PEPs exposure. Results represent mean ± SD. For statistical analysis, Wilcoxon sign ranked non-parametric test was performed.

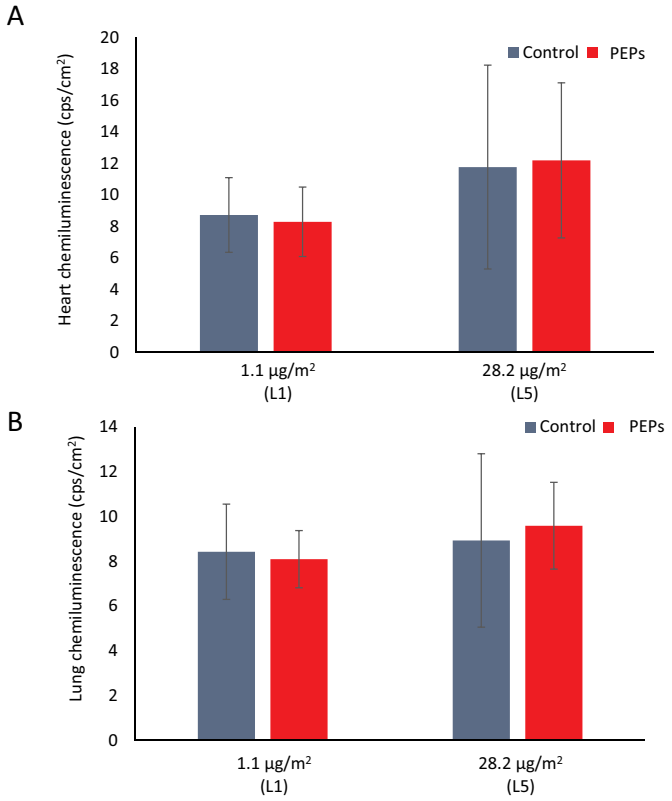

Fig. 7. *In situ* oxidative stress analysis. From the 2016 study, average relative (delta) signals in the (A) heart and (B) lung following exposure to PEPs and gaseous co-pollutants at the retention doses of 1.1 µg/m^2 (L5) and 28.2 µg/m^2 (L1). Results represent mean ± SD. For statistical analysis, Wilcoxon sign ranked non-parametric test was performed. P value * ≤ 0.05.

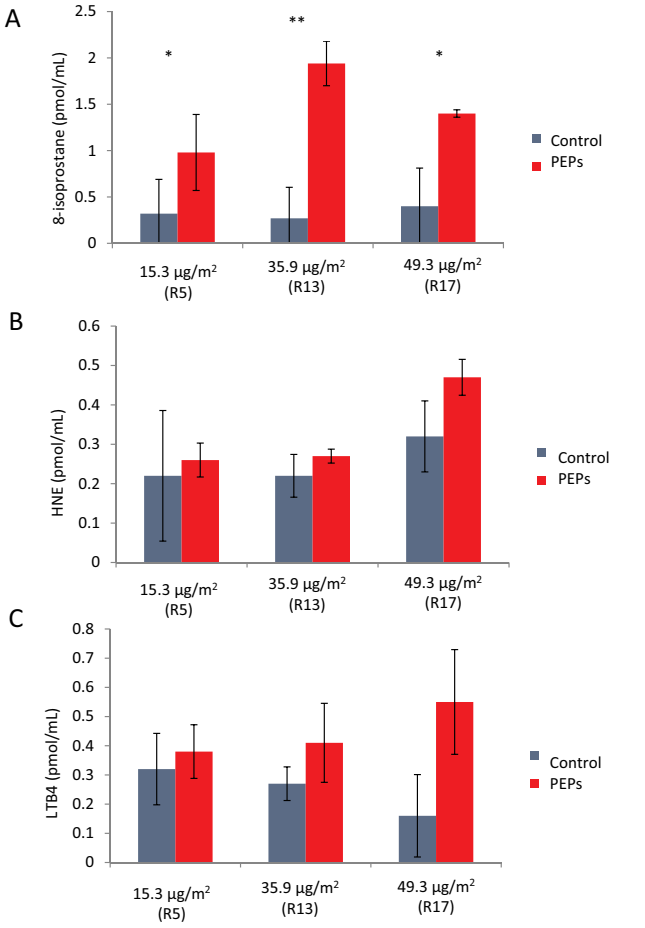

Fig. 8. PEPs induced inflammatory and oxidative stress biomarkers. Using LC-ESI-MS/MS, biomarkers of oxidative stress (A) 8-isoprostane and (B) 4-Hydroxy-2-nonenal (HNE), and of inflammation (C) leukotriene (LT) B4, were measured in the serum samples of rats exposed to PEPs and HEPA filtered air (control). Results showed an increase in the presence of 8-isoprostane, HNE and LTB4 markers representing oxidative stress and inflammation. Results represent mean ± SD. For statistical analysis, Wilcoxon sign ranked non-parametric test was performed. P value * ≤ 0.05 and ** ≤ 0.01.

difference in the chemiluminescence of the heart and lung of the animals exposed to PEPs was observed relative to controls (Fig. 7A and B).

3.8. Circulating biomarkers of lipid oxidation and inflammation leukotriene (LT) B4 in rat serum

8-Isoprostane and 4-HNE are well known markers of oxidative stress originating from free radical oxidation of arachidonic acid *in vivo* (Montuschi et al., 1999; Pelclova et al., 2017a, 2017b). LTB4 is an important, well-established inflammatory mediator generated from activated innate immune cells such as neutrophils, macrophages, and mast cells (Ohnishi et al., 2008). Elevated levels of LTB4 have been reported in various chronic diseases including allergic rhinitis, asthma, chronic obstructive pulmonary disease and rheumatoid arthritis (Sun et al., 2017; Ohnishi et al., 2008; Crooks et al., 1998).

Serum samples were collected from animals exposed to PEPs for 5, 13 and 17 days (R5, R13, and R17) in the 2017 study. Results showed that the 8-F2-α-isoprostane levels were significantly elevated in all the PEPs exposed animal groups as compared to the control animals (Fig. 8A). Elevation, although not statistically significant, in the levels of serum 8-F2-α-isoprostane could further be correlated to the increase in the retention dose of the PEPs (Fig. 8A). Similarly, the biomarkers 4-HNE (Fig. 8B) and LTB4 (Fig. 8C) were also observed to be elevated in the serum of the PEPs-exposed animals relative to their HEPA filtered air exposed controls. Elevation in the levels of the 4-HNE and LTB4 serum biomarkers was directly related to the increase in the retention dose of the PEPs (Fig. 8B and C). However, the elevated levels of 4-HNE and LTB4 were not found to be statistically significant, likely due to small sample size, exposure variability, and/or other compensatory mechanisms.

3.9. Determination of the 'No Observable Adverse Effect Level' (NOAEL), and the 'Lowest Observable Adverse Effect Level' (LOAEL)

The NOAEL and LOAEL are important concepts in toxicology used to derive regulatory guidance values for exposures in humans. According to the Environmental Protection Agency, NOAEL represents the highest exposure level at which there are no statistically or biologically significant increases in the frequency or severity of adverse effects between the exposed population and its appropriate control. Some effects may be produced at this level, but they are not considered to be adverse or precursors to adverse effects (EPA, 1995). Similarly, the LOAEL is defined as the lowest exposure level at which there are statistically or

biologically significant increases in the frequency or severity of adverse effects between the exposed population and its appropriate control (EPA, 1995).

In the present study, none to mild biological responses were observed in the PEPs-exposed animals using endpoints such as cytotoxicity, oxidative stress, lung injury, and inflammation. As shown in Supplemental Table S7, significant biological responses in the animals exposed to PEPs were detected between the retention doses of 28.2 μg/m^2 and 79.3 μg/m^2. Retention dose was used in determining the NOAEL and LOAEL for PEPs exposure. However, the deposition rate was also a factor involved in inducing pulmonary responses to PEPs exposure. Although variable responses in BALF LDH release were observed at equivalent retention doses of 28 μg/m^2, LDH release was closely related to the corresponding deposition rates (0.3 μg/h (L9) vs. 0.5 μg/h (L5)) (Supplemental Table S7).

Based upon the EPA definition, the NOAEL for PEPs exposure in rats was determined at the retention dose of 26.6 μg/m^2 (R9: deposition rate: 0.2 μg/h) and the LOAEL was determined at the retention dose of 28.2 μg/m^2 (L5: deposition rate of 0.4 μg/h) (Supplemental Table S7). Based upon biological endpoints and the aforementioned NOAEL (R9: 26.6 μg/m^2) and LOAEL (L5: 28.2 μg/m^2), the PEPs-exposed animal results were extrapolated to humans with the expectation for similar biological outcomes occurring from occupational exposure to PEPs. In humans, following pulmonary clearance, the NOAEL was calculated at retention dose of 4.7 mg/m^2 and LOAEL at 7.5 mg/m^2 for 8 h/day, 5 days a week and 3 weeks of exposure to PEPs (Supplemental Table S6) (Oller and Oberdorster, 2010).

It is worth noting that the NOAEL and LOAEL values for both rats and humans were extremely close to each other. This is due to the fact that lung responses to PEPs exposures were mild to none. The most sensitive biological endpoints in this study were found to be the circulating oxidative stress biomarkers, especially 8-isoprostane, which was elevated and statistically significant at all exposure endpoints (Fig. 8A).

4. Discussion

Increases in the application of engineered nanomaterials in the printing industry has made it important to understand the toxicity of PEPs in humans following inhalation exposure. Various studies have shown the particle diameter of laser PEPs to contain nanoparticles having diameters < 100 nm (Pirela et al., 2015; Namiki et al., 2006; He et al., 2007; Wensing et al., 2008; Morawska et al., 2009). In agreement with previous studies, we confirmed that PEPs produced by the laser printer used in our study emitted particles that were of nanoscale size with a median diameter of 46–67 nm. McGarry et al. (2011) reported that laser printers that emit nanoparticles are common in office workplaces with emitted particles ranging between 4.3×10^1 to 4×10^3 #/cm^3 during a normal working time of 8 h (Morawska et al., 2011). Compared to the McGarry and Morawska data, the overall airborne particle concentrations in our study were much higher and ranged from 4 to 21×10^5 #/cm^3. The number of PEPs emitted from the laser printer model B1 used in our study was close to that observed by Pirela et al. (2015) using laser printer B1 (Pirela et al., 2015). An important observation in our current study was the $PM_{0.1}$ exposure variability across different days due to wear and tear of the used printers. Similar variability in the peak emission of PEPs from office laser printers was also reported by McGarry et al. (2011).

It is worth noting that based on the real-time exposure data, the MPPD model estimated a variation in the lung deposited mass rate and deposited mass of PEPs in the deep lung of the exposed animals from the same exposure duration. For example, a 13-fold difference in the total lung deposited mass and deposition rate of PEPs (Supplemental Table S9) was estimated between exposure day 1 in 2016 (L1) and 2017 (R1). Higher PEPs deposited dose rates (0.4 μg/h, L5 *vs.* 0.3 μg/h, L9), at equal retention doses of approximately 28.2 μg/m^2, induced stronger biological responses (Supplemental Table S7). This outcome is in agreement with other studies that investigated the role of dose and dose rate for other nanoparticles (Baisch et al., 2014; Silva et al., 2014), and, illustrates the importance of dose rate as a dose metric rather than the static total lung deposited mass dose.

The overall picture from this three-week inhalation study is that no significant tissue injury was observed in histopathology examinations of the lungs and heart. This is in agreement with our previous *in vitro* studies with PEPs and *in vivo* instillation studies with a mouse model (Pirela et al., 2013, 2016a, 2016b). The complete genomic analysis and effects on cardiovascular system are underway and data will be reported in companion manuscripts in near future. In summary, modest lung injury and inflammation were observed in the deep lung, as indicated by the release of LDH and Hb, and an influx of inflammatory cells (neutrophils and lymphocytes) in PEPs-exposed animals. Mild LDH release was observed only at the PEPs retention doses of 28.2 and 79.3 μg/m^2, and presence of Hb was detected in the BALF at the PEPs retention dose of 70 μg/m^2. However, the levels of LDH release and Hb were relatively low and close to baseline. Low expression of other biomarkers of lung injury, namely peroxidase activity, indicated absence of extensive tissue injury in the PEPs-exposed animals relative to controls. Inflammatory mediators, such as cytokines (IL-1β, IL-12, IL-18, leptin), chemokines (MIP-1α, MIP-2,GRO/KC, CX3C, fractalkine), and growth factors (EFG) were found to be modestly (< 2–4 fold) up-regulated in the PEPs-exposed animals. Total GSH levels were moderately elevated, although not statistically significant, in the BALF of PEPs-exposed animals with retention doses of 252.1 μg/m^2 and deposition rates up to 1.2 μg/h. However, no ROS production was detected *in situ* in the lungs and heart tissues using *in vivo* chemiluminescence.

In the upper respiratory nasal region, no tissue damage was observed following measurement of biomarkers such as LDH, GSH and peroxidase activity. Few inflammatory mediators namely, IL-5, IL-12 and VEGF were found to be up-regulated beyond the PEPs retention dose of 28.2 μg/m^2. The results indicated mild response of the upper respiratory tract (*i.e.*, reflected in the NLF analyses) as compared to the lower respiratory tract BALF analyses in the PEPs-exposed animals.

In the present study, whole-body inhalation exposure of rats induced a mild release of pro- and anti-inflammatory mediators in the lower respiratory tract of the animals that could be related to the observed recruitment of neutrophils and lymphocytes. Under *in vitro* conditions, exposure of SAECs and an epithelial-endothelial cell co-culture system to PEPs ($PM_{0.1}$) was found to significantly up-regulate the expression of inflammatory mediators (Pirela et al., 2016a, 2016b; Sisler et al., 2015). Both IL-5 and IL-12 are involved in Th1 and Th2 type responses produced by innate and adaptive immune cells, such as macrophages, neutrophils and eosinophils. However, this study demonstrated a down-regulation of inflammatory mediators such as IL-1β, IFN-γ, leptin, and IL-13 in the nasal regions of PEPs-exposed animals. This was opposite to the response recorded in the nasal lavage from human volunteers exposed to copy-center particles for 6 h and may be related to interspecies variation in response to PEPs and physicochemical differences between PEPs and copy center particles (Khatri et al., 2013a, 2013b, 2013c, 2017).

Other cytokines and chemokines down-regulated in the PEPs-exposed animals were IL-17α and eotaxin, both of which are related to development of chronic inflammatory and allergic symptoms (Yao et al., 1995; Van Coillie et al., 1999). Absence of these markers indicates a moderate level of inflammatory response in the PEPs-exposed animals as also evidenced by the low influx of inflammatory cells such as eosinophils. The minor influx of neutrophils can be correlated to the presence of MIP-2 in the lower respiratory tract. MIP-2 has been observed to be activated in the presence of metal-based nanoparticles such as SiO_2 (Waters et al., 2009). Similarly, the presence of the CX3C chemokine (fractalkine), a chemoattractant for lymphocytes, in the pulmonary region of the PEPs-exposed animals can be correlated to the

mild increase in the population of lymphocytes observed in the BALF (Jones et al., 2010).

VEGF along with EGF are growth factors that have been associated with the development of many pulmonary diseases such as Chronic Obstructive Pulmonary Disease (COPD) and asthma (Zhang et al., 2018). VEGF has been found to be elevated (2–10 times) in the NLF obtained from human volunteers exposed to particles collected from a copier center (Khatri et al., 2013b). Similarly, *in vitro* studies with human monocytes and primary upper and small airways cells as well as an *in vivo* Balb/c mouse study demonstrated increases in VEGF levels in response to the same photocopy center particles (Pirela et al., 2013; Khatri et al., 2013c).

In a previous study, it was shown that PEPs contain PAHs, some of which have been categorized by Environmental Protection Agency as highly carcinogenic (Chalbot et al., 2017). In the current study, the main emphasis was on respiratory endpoints; additional endpoints reflecting adverse effects due exposures to carcinogenic PAHs should be included in future studies. Short-term exposure to a gavage dose (13 mg/kg) of the PAH benzo[*a*]pyrene resulted in reduced release of the inflammatory mediators IFN-γ and IL-4 in male and female C56BL/6 mice (Van den Berg et al., 2005). Reduction in IFN-γ has been directly related to the development of fibrosis as observed in asbestos exposures (Kikuchi et al., 2010). Previously, emissions from laser printers containing VOCs were found to be non-cytotoxic, but demonstrated the potential to induce genotoxicity and epigenetic changes under *in vitro* conditions in lung cells (Pirela et al., 2016a, 2016b; Tang et al., 2012).

In the systemic circulation, 8-isoprostane, the most significant biomarker of oxidative stress, is capable of inducing vasoconstriction of blood vessels and bronchi, lowering blood flow in the kidneys, and participating in the pathology of several diseases, such as asthma, COPD, atherosclerosis, and diabetes (Pelclova et al., 2017a, 2017b). In the present study, we found elevated levels of 8-isoprostane in the serum of PEPs-exposed animals, starting with day 1. While previous studies have correlated the increased levels of 8-isoprostane to metallic nanoparticle exposure and associated lipid peroxidation, PAHs present on the nanoparticles as condensed matter may equally contribute to increased levels of 8-isoprostane observed in the serum samples in our present study (Liou et al., 2017; Fahmy and Cormier, 2009; Ferguson et al., 2017). The up-regulation of this biomarker does reflect the possibility of systemic oxidative damage due to exposure to PEPs. However, further studies, such as a complete genomic profiling and biokinetics assessment, are needed to understand in detail the extent of the damage beyond the respiratory system as well as the different mechanisms by which 8-isoprostane is acting. Similarly, 4-HNE, another marker of oxidative stress was also elevated relative to controls albeit, it did not reach statistical significance. A similar trend to 4-HNE was observed for LBT4, which was elevated in all three exposure groups relative to controls, starting with day 1. Of note, the highest levels of LTB4 were measured after the first day of exposure, suggesting that animals may have developed compensatory mechanisms to reduce inflammation. LTB4 is an important biomarker, implicated in various lung diseases such as COPD and cystic fibrosis (Seggev et al., 1991; Ohnishi et al., 2008). The small sample size (n = 3 per group) is a likely reason for the statistically non-significant differences in 4-HNE and LTB4 levels. Another important consideration is that certain biomarker levels varied considerably with exposure time in control animals. For example, while levels of 8-isoprostane were steady in controls, they were elevated on day 13 for LTB4-4; peroxidase activity was elevated in the NLF of controls for the two retention doses of 252.1 μg/m^2 and 322.8 μg/m^2. There is no clear explanation for this observation, but it diminishes the significance of the general trends of increased concentration of some biomarkers with retained dose. The genome-scale profile of PEPs-exposed rats was completed to identify important gene signatures and potential mechanistic pathways of PEPs-induced toxicity. Such data will be published by the authors in a companion manuscript.

Our findings showed mild stimulation of innate immune cells, inflammation and systemic oxidative stress in PEPs-exposed animals with an estimated NOAEL at 26.5 μg/m^2 and a LOAEL at 28.2 μg/m^2 after lung clearance. Mild inflammatory responses are the underlying reason for the low variation between the NOAEL and LOAEL values. Other *in vitro* and *in vivo* studies have shown occurrences of respiratory cytotoxicity, oxidative stress and inflammation at higher concentrations of PEPs (summarized in Supplemental Table S10).

5. Conclusions

In conclusion, exposure to PEPs induced mild cytotoxicity, inflammation and oxidative stress in the respiratory region of Sprague-Dawley rats during this sub-acute 21-day whole-body inhalation exposure study. These responses were in the form of modest production of pro-inflammatory cytokines and chemokines, slight increase in white blood cells, and a modest increase in peroxidase activity and glutathione levels in the NLF and BALF of the exposed animals. The most significant responses observed were an increase in systemic oxidative stress (8-isoprostane and 4-HNE) and inflammation (LTB4) markers. The most significant responses observed were an increase in systemic oxidative stress (8-isoprostane and 4-HNE) and inflammation (LTB4) markers. Further research and studies are needed to provide additional insight into whether these effects are representative of an adaptive response following inhalation of PEPs. A genome-scale profile of the exposed animals will aid in identifying whether genetic profiles are modified by exposure to PEPs, and in turn, understanding the potential mechanism of toxicity of PEPs.

Although no significant adverse responses in the form of cytotoxicity and oxidative stress were recorded in the nasal region of the PEPs-exposed animals, mild inflammation was documented with the release of pro-inflammatory cytokines and chemokines beyond the PEPs retention dose of 35.9 μg/m^2 (R13). In the pulmonary region, based on the biological endpoints studied in BALF, no clear dose-response was observed in the PEPs-exposed animals. Histological and *in situ* ROS studies demonstrated no pathological effects from PEPs exposure to pulmonary and cardiac region of the exposed animals. Based on the measured biological responses to the PEPs, a concentration of 28.2 μg/m^2 was found to be the transition point from NOAEL to LOAEL for the respiratory endpoint studies.

Inflammatory cytokines and chemokines, and 8-isoprostane were determined as the most sensitive biomarkers of effect from exposure to PEPs.

Acknowledgements

The authors acknowledge funding for this study from National Institute for Occupational Safety and Health (NIOSH) and Consumer Protection Safety Commission (CPSC) (Grant No. 2012-M-51174), National Institute of Health (NIH) (Grant No. HL007118).

Appendix A. Supplementary data

Supplementary data to this article can be found online at https://doi.org/10.1016/j.impact.2019.100176.

References

Anjilvel, S., Asgharian, B., 1995. A multiple-path model of particle deposition in the rat lung. Fundam. Appl. Toxicol. 28 (1), 41–50.

Awodele, O., Akindele, A.J., Adebowale, G.O., Adeyemi, O.O., 2015. Polycyclic aromatic hydrocarbon, haematological and oxidative stress levels in commercial photocopier operators in Lagos, Nigeria. Ghana Med J. 49 (1), 37–43.

Baisch, B.L., Corson, N.M., Wade-Mercer, P., Gelein, R., Kennell, A.J., et al., 2014. Equivalent titanium dioxide nanoparticle deposition by intratracheal instillation and whole body inhalation: the effect of dose rate on acute respiratory tract inflammation. Part Fibre Toxicol. 11, 5.

Beck, B.D., Brain, J.D., Bohannon, D.E., 1982. An in vivo hamster bioassay to assess the

toxicity of particulates for the lungs. Toxicol. Appl. Pharmacol. 66 (1), 9–29.
Bello, D., Martin, J., Santeufemio, C., Sun, Q., et al., 2013. Physicochemical and morphological characterisation of nanoparticles from photocopiers: implications for environmental health. Nanotoxicology. 7 (5), 989–1003.
Chalbot, M.C.G., Pirela, S.V., Schifman, L., Kasaraneni, V., et al., 2017. Synergistic effects of engineered nanoparticles and organics released from laser printers using nano-enabled toners: potential health implications from exposures to the emitted organic aerosol. Environ. Sci.: Nano 4, 2144–2156.
Crooks, S.W., Stockley, R.A., Leukotriene, B4., 1998. Int J Biochem Cell Biol. 30 (2), 173–178.
DeLoid, G.M., Wang, Y., Kapronezai, K., Lorente, L.R., Zhang, R., Pyrgiotakis, G., Konduru, N.V., Ericsson, M., White, J.C., De La Torre-Roche, R., Xiao, H., McClements, D.J., Demokritou, P., 2017. An integrated methodology for assessing the impact of food matrix and gastrointestinal effects on the biokinetics and cellular toxicity of ingested engineered nanomaterials. Part Fibre Toxicol. 14 (1), 40.
DeLoid, G.M., Sohal, I.S., Lorente, L.R., Molina, R.M., Pyrgiotakis, G., Stevanovic, A., Zhang, R., McClements, D.J., Geitner, N.K., Bousfield, D.W., Ng, K.W., Loo, S.C.J., Bell, D.C., Brain, J., Demokritou, P., 2018. Reducing intestinal digestion and absorption of fat using a nature-derived biopolymer: interference of triglyceride hydrolysis by nanocellulose. ACS Nano 12 (7), 6469–6479.
Doumas, B.T., Watson, W.A., Biggs, H.G., 1971. Albumin standards and the measurement of serum albumin with bromocresol green. Clin. Chim. Acta 31 (1), 87–96.
Elango, N., Kasi, V., Vembhu, B., Poornima, J.G., 2013. Chronic exposure to emissions from photocopiers in copy shops causes oxidative stress and systematic inflammation among photocopier operators in India. Environ. Health 12 (1), 78.
Eleftheriadou, M., Pyrgiotakis, G., Demokritou, P., 2017. Nanotechnology to the rescue: using nano-enabled approaches in microbiological food safety and quality. Curr. Opin. Biotechnol. https://doi.org/10.1016/j.copbio.2016.11.012.
Fahmy, B., Cormier, S.A., 2009. Copper oxide nanoparticles induce oxidative stress and cytotoxicity in airway epithelial cells. Toxicol. in Vitro 23 (7), 1365–1371.
Ferguson, K.K., McElrath, T.F., Pace, G.G., Weller, D., Zeng, L., Pennathur, S., Cantonwine, D.E., Meeker, J.D., 2017. Urinary polycyclic aromatic hydrocarbon metabolite associations with biomarkers of inflammation, angiogenesis, and oxidative stress in pregnant women. Environ Sci Technol. 51, 4652–4660.
Jarabek, A.M., Asgharian, B., Miller, F.J., 2005. Dosimetric adjustments for interspecies extrapolation of inhaled poorly soluble particles (PSP). Inhal. Toxicol. 17 (7–8), 317–334.
Jones, B.A., Beamer, M., Ahmed, S., 2010. Fractalkine/CX3CL1: a potential new target for inflammatory diseases. Mol. Interv. 10 (5), 263–270.
Karimi, A., Eslamizad, S., Mostafaee, M., Momeni, Z., et al., 2016. Restrictive pattern of pulmonary symptoms among photocopy and printing workers: a retrospective cohort study. J Res Health Sci. 16 (2), 81–84.
Khatri, M., Bello, D., Gaines, P., Martin, J., et al., 2013a. Nanoparticles from photocopiers induce oxidative stress and upper respiratory tract inflammation in healthy volunteers. Nanotoxicology 7 (5), 1014–1027.
Khatri, M., Bello, D., Pal, A.K., Cohen, J.M., et al., 2013b. Evaluation of cytotoxic, genotoxic and inflammatory responses of nanoparticles from photocopiers in three human cell lines. Part Fibre Toxicol. 10, 42.
Khatri, M., Bello, D., Pal, A.K., Woskie, S., et al., 2013c. Toxicological effects of PM 0.25-2.0 particles collected from a photocopy center in three human cell lines. Inhal. Toxicol. 25, 621–632.
Khatri, M., Bello, D., Martin, J., Bello, A., et al., 2017. Chronic upper airway inflammation and systemic oxidative stress from nanoparticles in photocopier operators: mechanistic insights. NanoImpact. 5, 133–145.
Kikuchi, N., Ishii, Y., Morishima, Y., Yageta, Y., et al., 2010. Nrf2 protects against pulmonary fibrosis by regulating the lung oxidant level and Th1/Th2 balance. Respir. Res. 11, 31.
Konduru, N.V., Murdaugh, K.M., Sotiriou, G.A., Donaghey, T.C., et al., 2014. Bioavailability, distribution and clearance of tracheally-instilled and gavaged uncoated or silica-coated zinc oxide nanoparticles. Part Fibre Toxicol. 11, 44.
Kreyling, W.G., Holzwarth, U., Haberl, N., Kozempel, J., et al., 2017. Quantitative biokinetics of titanium dioxide nanoparticles after intratracheal instillation in rats: part 3. Nanotoxicology. 11 (4), 454–464.
Liou, S.H., Wu, W.T., Liao, H.Y., Chen, C.Y., Tsai, C.Y., Jung, W.T., Lee, H.L., 2017. Global DNA methylation and oxidative stress biomarkers in workers exposed to metal oxide nanoparticles. J. Hazard. Mater. 331, 329–335.
Lu, X., Miousse, I.R., Pirela, S.V., Melnyk, S., et al., 2015. Short-term exposure to engineered nanomaterials affects cellular epigenome. Nanotoxicology. 10 (2), 1–11.
Lu, X., Miousse, I.R., Pirela, S.V., Moore, J.K., et al., 2016. In vivo epigenetic effects induced by engineered nanomaterials: a case study of copper oxide and laser printer-emitted engineered nanoparticles. Nanotoxicology. 10 (5), 629–639.
Martin, J., Bello, D., Bunker, K., Shafer, M., et al., 2015. Occupational exposure to nanoparticles at commercial photocopy centers. J. Hazard. Mater. 298, 351–360.
McClements, D.J., DeLoid, G., Pyrgiotakis, G., Shatkin, J.A., Demokritou, P., 2016. The role of the food matrix and gastrointestinal tract in the assessment of biological properties of ingested engineered nanomaterials (iENMs): state of the science and knowledge gaps. NanoImpact. 3-4, 47–57.
McGarry, P., Morawska, L., He, C., Jayaratne, R., Falk, M., Tran, Q., Wang, H., 2011. Exposure to particles from laser printers operating within office workplaces. Environ Sci Technol. 45 (15), 6444–6452.
Miller, M.R., Raftis, J.B., Langrish, J.P., McLean, S.G., et al., 2017. Inhaled nanoparticles accumulate at sites of vascular disease. ACS Nano 11 (5), 4542–4552.
Montuschi, P., Corradi, M., Ciabattoni, G., Nightingale, J., et al., 1999. Increased 8-iso-prostane, a marker of oxidative stress, in exhaled condensate of asthma patients. Am. J. Respir. Crit. Care Med. 160 (1), 216–220.
Morawska, L., He, C., Johnson, G., Jayaratne, R., Salthammer, T., Wang, H., Uhde, E., Bostrom, T., Modini, R., Ayoko, G., Mcgarry, P., Wensing, M., 2009. An investigation into the characteristics and formation mechanisms of particles originating from the operation of laser printers. Environ. Sci. Technol. 43, 1015–1022.
Morfeld, P., Bruch, J., Levy, L., Ngiewih, Y., et al., 2015. Translational toxicology in setting occupational exposure limits for dusts and hazard classification - a critical evaluation of a recent approach to translate dust overload findings from rats to humans. Part Fibre Toxicol. 12, 3.
Namiki, N., Otani, Y., Fujii, S., Kagi, N., 2006. Characterisation of emission of ultrafine particles from office printers. J. Aerosol Res. 21, 59–65 (Jap).
Ohnishi, H., Miyahara, N., Gelfand, E.W., 2008. The role of leukotriene B(4) in allergic diseases. Allergol. Int. 57 (4), 291–298.
Oller, A.R., Oberdorster, G., 2010. Incorporation of particle size differences between animal studies and human workplace aerosols for deriving exposure limit values. Regulatory Toxicol Pharma. 57 (2–3), 181–194.
Pal, A.K., Watson, C.Y., Pirela, S.V., Singh, D., et al., 2015. Linking exposures of particles released from nano-enabled products to toxicology: an integrated methodology for particle sampling, extraction, dispersion, and dosing. Toxicol. Sci. 146, 321–333.
Pelclova, D., Zdimal, V., Kacer, P., Zikova, N., Komarc, M., Fenclova, Z., Vlckova, S., Schwarz, J., Makeš, O., Syslova, K., Navratil, T., Turci, F., Corazzari, I., Zakharov, S., Bello, D., 2017a. Markers of lipid oxidative damage in the exhaled breath condensate of nano TiO_2 production workers. Nanotoxicology. 11 (1), 52–63.
Pelclova, D., Zdimal, V., Kacer, P., Komarc, M., et al., 2017b. Markers of lipid oxidative damage among office workers exposed intermittently to air pollutants including nanoTiO_2 particles. Rev. Environ. Health 32 (1–2), 193–200.
Pinkerton, K., Gehr, P., Castañeda, A., Crapo, J.D., 2015. Architecture and cellular composition of the air–blood tissue barrier. In: Parent, R.A. (Ed.), Comparative Biology of the Normal Lung, 2nd ed. pp. 105–117.
Pirela, S., Molina, R., Watson, C., Cohen, J.M., Bello, D., Demokritou, P., Brain, J., 2013. Effects of copy center particles on the lungs: a toxicological characterization using a Balb/c mouse model. Inhal. Toxicol. 25 (9), 498–508.
Pirela, S.V., Pyrgiotakis, G., Bello, D., Thomas, T., Castranova, V., Demokritou, P., 2014. Development and characterization of an exposure platform suitable for physico-chemical, morphological and toxicological characterization of printer-emitted particles (PEPs). Inhal. Toxicol. 26 (7), 400–408.
Pirela, S.V., Sotiriou, G.A., Bello, D., Shafer, M., et al., 2015. Consumer exposures to laser printer emitted engineered nanoparticles: a case study of life-cycle implications from nano-enabled products. Nanotoxicology. 9 (6), 760–768.
Pirela, S.V., Lu, X., Miousse, I., Sisler, J.D., et al., 2016a. Effects of intratracheally instilled laser printer-emitted engineered nanoparticles in a mouse model: a case study of toxicological implications from nanomaterials released during consumer use. NanoImpact. 1, 1–8.
Pirela, S.V., Miousse, I.R., Lu, X., Castranova, V., Thomas, T., Qian, Y., Bello, D., Kobzik, L., Koturbash, I., Demokritou, P., 2016b. Effects of laser printer-emitted engineered nanoparticles on cytotoxicity, chemokine expression, reactive oxygen species, DNA methylation, and DNA damage: a comprehensive in vitro analysis in human small airway epithelial cells, macrophages, and lymphoblasts. Environ. Health Perspect. 124 (2), 210–219.
Pirela, S.V., Martin, J., Bello, D., Demokritou, P., 2017. Nanoparticle exposures from nano-enabled toner-based printing equipment and human health: state of science and future research needs. Crit. Rev. Toxicol. 47 (8), 678–704.
Pyrgiotakis, G., Vedantam, P., Cirenza, C., McDevitt, J., Eleftheriadou, M., Leonard, S.S., Demokritou, P., 2016. Optimization of a nanotechnology based antimicrobial platform for food safety applications using Engineered Water Nanostructures (EWNS). Sci. Rep. 6, 21073.
Schoepf, J.J., Bi, Y., Kidd, J., Herckes, P., Westerhoff, P., 2017. Detection and dissolution of needle-like hydroxyapatite nanomaterials in infant formula. NanoImpact 5, 22–28.
Scungio, M., Vitanza, T., Stabile, L., Buonanno, G., Morawska, L., 2017. Characterization of particle emission from laser printers. Sci. Total Environ. 586, 623–630.
Servin, A.D., White, J.C., 2016. Nanotechnology in agriculture: next steps for understanding engineered nanoparticle exposure and risk. NanoImpact 1, 9–12.
Silva, R.M., Doudrick, K., Franzi, L.M., TeeSy, C., et al., 2014. Instillation versus inhalation of multiwalled carbon nanotubes: exposure-related health effects, clearance, and the role of particle characteristics. ACS Nano 8 (9), 8911–8931.
Singh, D., Schifman, L.A., Watson-Wright, C., Sotiriou, G.A., et al., 2017. Nanofiller presence enhances polycyclic aromatic hydrocarbon (PAH) profile on nanoparticles released during thermal decomposition of nano-enabled thermoplastics: potential environmental health implications. Environ Sci Technol. 51 (9), 5222–5232.
Sisler, J.D., Pirela, S.V., Friend, S., Farcas, M., et al., 2015. Small airway epithelial cells exposure to printer-emitted engineered nanoparticles induces cellular effects on human microvascular endothelial cells in an alveolar-capillary co-culture model. Nanotoxicology. 9 (6), 769–779.
Sohal, I.S., Cho, Y.K., O'Fallon, K.S., Gaines, P., Demokritou, P., Bello, D., 2018a. Dissolution behavior and biodurability of ingested engineered nanomaterials in the gastrointestinal environment. ACS Nano 12 (8), 8115–8128.
Sohal, I.S., O'Fallon, K.S., Gaines, P., Demokritou, P., Bello, D., 2018b. Ingested engineered nanomaterials: state of science in nanotoxicity testing and future research needs. Part Fibre Toxicol. 15, 29.
Sotiriou, G.A., Diaz, E., Long, M.S., Godleski, J., et al., 2012. A novel platform for pulmonary and cardiovascular toxicological characterization of inhaled engineered nanomaterials. Nanotoxicology 6 (6), 680–690.
Sotiriou, G.A., Singh, D., Zhang, F., Wohlleben, W., Chalbot, M.G., Kavouras, I.G., Demokritou, P., 2015. An integrated methodology for the assessment of environmental health implications during thermal decomposition of nano-enabled products. Environ Sci Nano. 2, 262–272.
Sotiriou, G.A., Singh, D., Zhang, F., Chalbot, M.G., Spielman-Sun, E., Hoering, L., Kavouras, I.G., Lowry, G.V., Wohlleben, W., Demokritou, P., 2016. Thermal

decomposition of nano-enabled thermoplastics: possible environmental health and safety implications. J. Hazard. Mater. 305, 87–95.
Sun, M., Wang, R., Han, Q., 2017. Inhibition of leukotriene B4 receptor 1 attenuates lipopolysaccharide-induced cardiac dysfunction: role of AMPK-regulated mitochondrial function. Sci. Rep. 7, 44352.
Syslová, K., Kačer, P., Kuzma, M., Najmanová, V., Fenclová, et al., 2009. Rapid and easy method for monitoring oxidative stress markers in body fluids of patients with asbestos or silica-induced lung diseases. J. Chromatogr. B 877 (24), 2477–2486.
Tang, T., Gminski, R., Könczöl, M., Modest, C., Armbruster, B., Mersch-Sundermann, V., 2012. Investigations on cytotoxic and genotoxic effects of laser printer emissions in human epithelial A549 lung cells using an air/liquid exposure system. Environ. Mol. Mutagen. 53 (2), 125–135 (Mar).
Theegarten, D., Boukercha, S., Philippou, S., Anhenn, O., 2010. Submesothelial deposition of carbon nanoparticles after toner exposition: case report. Diagn. Pathol. 5, 77.
Van Coillie, E., Van Damme, J., Opdenakker, G., 1999. The MCP/eotaxin subfamily of CC chemokines. Cytokine Growth Factor Rev. 10 (1), 61–86.
Van den Berg, F.A., Baken, K.A., Vermeulen, J.P., Gremmer, E.R., et al., 2005. Use of the local lymph node assay in assessment of immune function. Toxicology. 211 (1–2), 107–114.
Vaze, N., Jiang, Y., Mena, L., Zhang, Y., Bello, D., Leonard, S.S., Morris, A.M., Eleftheriadou, M., Pyrgiotakis, G., Demokritou, P., 2018. An integrated electrolysis - electrospray - ionization antimicrobial platform using Engineered Water Nanostructures (EWNS) for food safety applications. Food Control 85, 151–160.
Waters, K.M., Masiello, L.M., Zangar, R.C., Tarasevich, B.J., et al., 2009. Macrophage responses to silica nanoparticles are highly conserved across particle sizes. Toxicol. Sci. 107 (2), 553–569.
Watson-Wright, C., Singh, D., Demokritou, P., 2017. Toxicological implications of released particulate matter during thermal decomposition of nano-enabled thermoplastics. NanoImpact. 5, 29–40.
Wensing, M., Schripp, T., Uh, E., Salthammer, T., 2008. Ultra-fine particles release from hardcopy devices: sources, real-room measurements and efficiency of filter accessories. Sci. Total Environ. 407, 418–427.
Wohlleben, W., Neubauer, N., 2016. Quantitative rates of release from weathered nanocomposites are determined across 5 orders of magnitude by the matrix, modulated by the embedded nanomaterial. NanoImpact. 1, 39–45.
Yang, C.-Y., Haung, Y.-C., 2008. A cross-sectional study of respiratory and irritant health symptoms in photocopier workers in Taiwan. J Toxicol Environ Health A. 71 (19), 1314–1317.
Yao, Z., Painter, S.L., Fanslow, W.C., Ulrich, D., et al., 1995. Human IL-17: a novel cytokine derived from T cells. J. Immunol. 155 (12), 5483–5486.
Yao, M., McClements, D.J., Zhao, F., Craig, R.W., Xiao, H., 2017. Controlling the gastrointestinal fate of nutraceutical and pharmaceutical-enriched lipid nanoparticles: from mixed micelles to chylomicrons. NanoImpact. 5, 13–21.
Zhang, X., Bao, W., Fei, X., Zhang, Y., et al., 2018. Progesterone attenuates airway remodeling and glucocorticoid resistance in a murine model of exposing to ozone. Mol. Immunol. 96, 69–77.